Detecting faults and channels while enhancing seismic structural and stratigraphic features

Xinming Wu[1] and Zhenwei Guo[2]

Abstract

A 3D seismic image contains structural and stratigraphic features such as reflections, faults, and channels. When smoothing such an image, we want to enhance all of these features so that they are easier to interpret. Most smoothing methods aim to enhance reflections but may blur faults and channels in the image. A few methods smooth seismic reflections while preserving faults and channel boundaries. However, it has not well-discussed to smooth simultaneously along the seismic reflections and channels, which are linear features apparent within dipping reflections. In addition, to interpret faults and channels, extra steps are required to compute attributes or mappings of faults and channels from a seismic image. Such fault and channel attributes are often sensitive to noise because they are typically computed as discontinuities of seismic reflections. In this paper, we have developed methods to simultaneously enhance seismic reflections, faults, and channels while obtaining mappings of the faults and channels. In these methods, we first estimate the orientations of the reflections, faults, and channels directly in a seismic image. We then use the estimated orientations to control the smoothing directions in an efficient iterative diffusion scheme to smooth a seismic image along the reflections and channels. In this iterative scheme, we also efficiently compute mappings of faults and channels, which are used to control smoothing extents in the diffusion to stop smoothing across them. This diffusion scheme iteratively smooths a seismic image along reflections and channels while updating the mappings of faults and channels. By doing this, we will finally obtain an enhanced seismic image (with enhanced reflections and channels and sharpened faults) and cleaned mappings of faults and channels (discontinuities related to noise are cleaned up). We have examined the methods using 2D and 3D real seismic images.

Introduction

Seismic interpretation often includes extracting structural and stratigraphic features such as horizons, faults, and channels from a seismic image (Wu and Hale, 2016b). The seismic horizons can be directly extracted from a seismic image by following reflections, which are dominant linear (2D) or planar (3D) features in the seismic image (Wu and Hale, 2015). The seismic faults and channels are recognized as the lateral discontinuities of reflections in a seismic image (Gersztenkorn and Marfurt, 1999; Chopra and Marfurt, 2007). In a 3D seismic image, channels are also spatially apparent as linear features that are aligned within dipping reflections (Wu, 2017). To extract seismic faults and channels, we often need to compute an extra attribute image from a seismic image so that the faults and channels are the most prominent features in the attribute image (Wu and Hale, 2016a; Wu, 2017).

In practice, such structural and stratigraphic features may not be obvious to track in a seismic image because of noise or limitations in seismic imaging methods. Therefore, a helpful step before seismic interpretation is to first enhance the structural and stratigraphic features in the seismic image so that the reflections are more continuous in areas away from faults and channels, the reflection discontinuities near faults and channels are more obvious, and the channels are spatially more continuous along dipping horizons or reflections. Some methods (e.g., Bakker et al., 1999; Fehmers and Höcker, 2003; Lavialle et al., 2007; Hale, 2009, 2011; Liu et al., 2010) have been proposed to enhance seismic reflections while preserving reflection discontinuities near faults and channel boundaries. To enhance the linear or planar reflections, most authors (Fehmers and Höcker, 2003; Lavialle et al., 2007; Hale, 2009) construct structure-oriented filters to smooth a seismic image along reflections by using anisotropic diffusion (Weickert, 1997, 1999). Some other authors construct structure-oriented filters using the steered Kuwahara filter (Bakker et al., 1999; AlBinHassan et al., 2006), plane-wave prediction (Liu et al., 2010), and steered bilateral filter

[1]The University of Texas at Austin, Bureau of Economic Geology, Austin, Texas, USA.
[2]Central South University, Changsha, China. E-mail: guozhenwei@csu.edu.cn.

Manuscript received by the Editor 21 September 2017; revised manuscript received 6 July 2018; published ahead of production 18 September 2018; published online 21 December 2018. This paper appears in *Interpretation*, Vol. 7, No. 1 (February 2019); p. T155–T166, 14 FIGS., 3 TABLES.
http://dx.doi.org/10.1190/INT-2017-0174.1.

(Hale, 2011). To preserve reflection discontinuities near faults, all the methods require computing some fault image to stop the smoothing at the faults. To preserve computational efficiency, some authors (Bakker et al., 1999; Hale, 2009) do not update the fault image during the smoothing. However, such a fault image is often sensitive to noise, some other authors (Fehmers and Höcker, 2003; Lavialle et al., 2007; Liu et al., 2010; Hale, 2011) therefore prefer to iteratively update the fault image to obtain a more accurate detection of faults and to better preserve faults during the smoothing.

Although structure-oriented smoothing methods have been proposed to enhance seismic reflections while preserving faults and channel boundaries, it is not discussed to simultaneously enhance or smooth along seismic stratigraphic features such as channels. In addition, the efficiency of the previous structure-oriented smoothing methods can be further improved. In this paper, we discuss fast cyclic explicit diffusion methods to simultaneously enhance reflections, faults, and channels in a seismic image while computing enhanced images of faults and channels. In the methods, we first estimate the orientations of reflections, faults, and channels from a seismic image. We also compute fault and channel mappings from the seismic image and apply fault- and channel-oriented smoothing to enhance the fault and channel features in these mappings. We then use the orientations of reflections and channels to control the smoothing directions in an iterative diffusion scheme to smooth along reflections and channels in the seismic image. The fault and channel mappings are used to control the smoothing extents in the diffusion scheme so that the smoothing is performed along reflections and channels but not across faults and channels. In the diffusion scheme, we iteratively update the fault and channel mappings together with the seismic image. The finally updated fault and channel images will display enhanced faults and channels, whereas the finally updated seismic image will display enhanced reflections, channels, and sharpen discontinuities near faults and channel boundaries. To accelerate the diffusion, we use the fast explicit diffusion (FED) method proposed by Grewenig et al. (2010) and Weickert et al. (2016), which requires fewer iterations than the conventional explicit diffusions schemes. We demonstrate the proposed methods using 2D and 3D examples with many faults and channels.

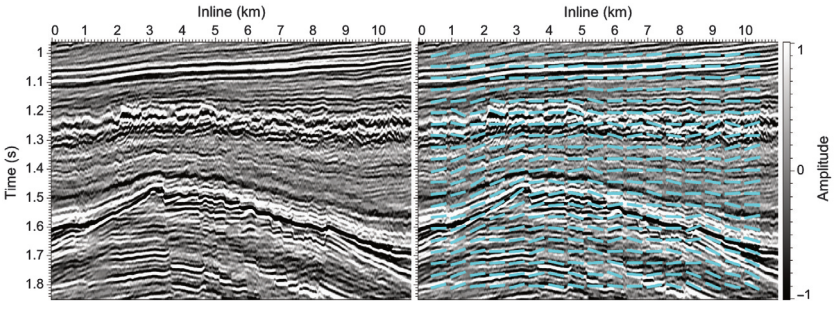

Figure 1. (a) A 2D seismic image is displayed with the (b) eigenvectors **v** (the cyan segments) of structure tensors.

Structural and stratigraphic orientations

Several methods, such as the structure tensor (Van Vliet and Verbeek, 1995; Weickert, 1997; Fehmers and Höcker, 2003), coherence scanning (Marfurt, 2006), plane-wave destruction (Fomel, 2002), and dynamic image warping (Arias, 2016), have been proposed to estimate seismic reflection orientations or slopes. However, the latter three methods are not applicable to estimate orientations of seismic stratigraphic features such as channels that are generally aligned within dipping reflections. In this paper, we use the structure tensor method to estimate orientations of structural features (reflections) and stratigraphic features (channels).

Structure tensors

A structure tensor $\mathbf{T}$ at each seismic image sample can be constructed as a smoothed outer product of image gradient $\mathbf{g}$: $\mathbf{T} = \langle \mathbf{g}\mathbf{g}^{\top} \rangle$, where $\langle \cdot \rangle$ denotes the smoothing for each element of the outer product or structure tensor. This smoothing, often implemented as a Gaussian filter, helps to construct structure tensors with stable estimations of seismic structural and stratigraphic orientations.

For each image sample in a 2D image, a structure tensor $\mathbf{T}$ is a 2×2 symmetric positive-semidefinite matrix

$$\mathbf{T} = \langle \mathbf{g}\mathbf{g}^{\top} \rangle = \begin{bmatrix} \langle g_1 g_1 \rangle & \langle g_1 g_2 \rangle \\ \langle g_1 g_2 \rangle & \langle g_2 g_2 \rangle \end{bmatrix}, \tag{1}$$

where $\mathbf{g} = [g_1 g_2]$ represent the 2D image gradients with first derivatives computed in the vertical (g_1) and horizontal (g_2) directions and $\langle \cdot \rangle$ denotes the smoothing of whatever is inside the angle brackets. As shown by Fehmers and Höcker (2003), the seismic reflection orientation at each image sample can be estimated from the eigendecomposition of the structure tensor $\mathbf{T}$ at that sample

$$\mathbf{T} = \lambda_u \mathbf{u}\mathbf{u}^{\top} + \lambda_v \mathbf{v}\mathbf{v}^{\top}, \tag{2}$$

where λ_u and λ_v are the eigenvalues corresponding to eigenvectors $\mathbf{u}$ and $\mathbf{v}$ of $\mathbf{T}$. If we label the eigenvalues $\lambda_u \geq \lambda_v \geq 0$, then the corresponding eigenvectors $\mathbf{u}$ will be perpendicular to locally linear features (seismic reflections) in an image and the eigenvectors $\mathbf{v}$ will be parallel to such features. Figure 1a shows a 2D seismic image, and the cyan segments in Figure 1b represent the eigenvectors $\mathbf{v}$ that are aligned with the seismic reflections in the image. Although we display the eigenvectors $\mathbf{v}$ only at some image samples in Figure 1b, we actually compute eigenvectors $\mathbf{u}$ and $\mathbf{v}$ for all image samples from the eigendecomposition of 2D structure tensors.

For each sample in a 3D image, a structure tensor $\mathbf{T}$ is a 3×3 symmetric positive-semidefinite matrix

$$\mathbf{T} = \langle \mathbf{g}\mathbf{g}^{\top} \rangle = \begin{bmatrix} \langle g_1 g_1 \rangle & \langle g_1 g_2 \rangle & \langle g_1 g_3 \rangle \\ \langle g_1 g_2 \rangle & \langle g_2 g_2 \rangle & \langle g_2 g_3 \rangle \\ \langle g_1 g_3 \rangle & \langle g_2 g_3 \rangle & \langle g_3 g_3 \rangle \end{bmatrix}, \tag{3}$$

where g_1, g_2, and g_3 are the three components of an image gradient vector $\mathbf{g}$ computed at a 3D image sample. The eigendecomposition of such a 3D structure tensor is as follows:

$$\mathbf{T} = \lambda_u \mathbf{u}\mathbf{u}^{\top} + \lambda_v \mathbf{v}\mathbf{v}^{\top} + \lambda_w \mathbf{w}\mathbf{w}^{\top}, \tag{4}$$

where λ_u, λ_v, and λ_w are the eigenvalues corresponding to orthogonal eigenvectors $\mathbf{u}$, $\mathbf{v}$, and $\mathbf{w}$, respectively. If we label the eigenvalues $\lambda_u \geq \lambda_v \geq \lambda_w \geq 0$, then the corresponding eigenvectors $\mathbf{u}$ will be parallel to directions in which the image features vary most significantly, whereas the eigenvectors $\mathbf{w}$ will be parallel to directions in which the image features vary the least significantly. In a 3D seismic image, the eigenvectors $\mathbf{u}$ are locally perpendicular to seismic reflections, whereas the eigenvectors $\mathbf{w}$ are locally parallel to seismic stratigraphic features (channels) that are aligned within the reflections (Hale, 2009). The eigenvectors $\mathbf{u}$ are orthogonal to seismic reflections and stratigraphic features. Figure 2 displays the three eigenvectors on a stratigraphic surface that can be extracted from a 3D seismic image by following seismic reflections. As shown in Figure 2, the eigenvector $\mathbf{u}$ is normal to the surface, whereas eigenvectors $\mathbf{v}$ and $\mathbf{w}$ lie within a local plane of the surface and are laterally perpendicular and parallel to the channel, respectively.

With the eigenvectors derived from 2D or 3D structure tensors, we are able to design anisotropic filters that smooth along seismic structural and stratigraphic features. In this paper, we construct such a structure- and stratigraphy-oriented smoothing filter with anisotropic diffusion (e.g., Weickert, 1997, 1999; Ma and Plonka, 2007; Plonka and Ma, 2008). Such anisotropic diffusion filters are based on a physical heat diffusion process, but the diffusion is steered by a tensor field that may be constructed from the eigenvectors of structure tensors. Some authors (Fehmers and Höcker, 2003; Hale, 2009) have applied such anisotropic diffusion filters to enhance seismic reflections while preserving faults. However, these anisotropic diffusion filters may blur seismic stratigraphic features such as channels by smoothing along seismic reflections. Moreover, the fault images used to preserve faults in these methods can be further enhanced by applying approximate fault-oriented smoothing to the images. Figure 3a shows a smoothed image computed by applying the structure-oriented smoothing method, proposed by Hale (2009), to the original seismic image in Figure 1. We observe that this method works pretty well to enhance the seismic reflections but also remove the reflection discontinuities related to faults as shown in the smoothed image (Figure 3a) and the input-output difference image (Figure 3b). To preserve the faults within the smoothed image, a fault attribute image such as coherence is required as an extra input for the method as discussed by Hale (2009). In addition, although this method requires only 0.086 s to compute this 2D smoothed image by using an eight-core computer, the computational efficiency can still be significantly improved.

In this paper, we will discuss anisotropic diffusion filters to simultaneously enhance reflections, faults, and channels in a seismic image and at the same time compute enhanced mappings of faults and channels. We solve the anisotropic diffusion using the FED method proposed by Grewenig et al. (2010) and Weickert et al. (2016), which is significantly more efficient than the previous structure-oriented filters (Fehmers and Höcker, 2003; Hale, 2009) used in seismic image smoothing.

Fast explicit diffusion

The anisotropic diffusion can be implemented explicitly using an iterative scheme (Weickert, 1999; Fehmers and Höcker, 2003) or implicitly by solving a large linear system (Hale, 2009). In this paper, we use the FED method (Grewenig et al., 2010; Weickert et al., 2016) to more efficiently solve the anisotropic diffusion filters. Then, we will explain the FED method using a simple 1D homogeneous diffusion problem.

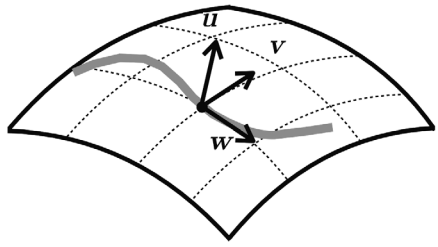

Figure 2. Eigenvectors $\mathbf{u}$, $\mathbf{v}$, and $\mathbf{w}$ of a 3D structure tensor are displayed on a stratigraphic surface with a channel. The vector $\mathbf{u}$ is orthogonal to the surface and the channel. The vectors $\mathbf{v}$ and $\mathbf{w}$ lie within the local plane of the surface and are laterally perpendicular and parallel to the channel, respectively.

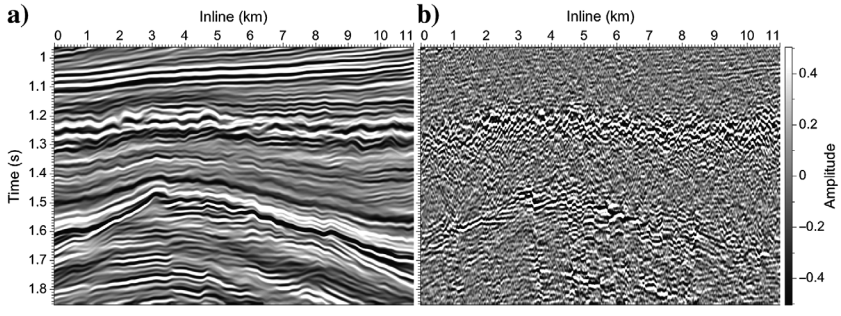

Figure 3. (a) Smoothed image computed by Hale's method (computational time: 0.086 s). (b) Input-output difference.

1D linear diffusion

A 1D homogeneous diffusion of a function $g(x;t)$ can be expressed as

$$\frac{\partial g(x;t)}{\partial t} = \frac{\partial}{\partial x}\frac{\partial g(x;t)}{\partial x}. \tag{5}$$

Let h denote the spatial mesh size and τ ($\tau > 0$) denote the time step size, and then the discretization of the above equation at a spatial-time-grid point $(x_i;t_k)$ with $x_i := (i-(1/2))h$ and $t_k := k\tau$ can be formulated as

$$g(x_i;t_{k+1}) = (I+\tau\Delta)g(x_i;t_k), \tag{6}$$

where I is the identity operator and Δ represents the discrete second derivative operator.

Iteratively solving the above diffusion equation 6 with g_i is equivalent in applying a Gaussian smoothing filter to the discretized sequence g_i (Weickert, 1997; Grewenig et al., 2010). This diffusion process with stop time $t_k = \sigma^2/2$ yields the comparable smoothing extent of a Gaussian smoothing filter with the half-width σ (Weickert, 1998). Because the stability restriction for the time step size is $\tau \le h^2/2$, a diffusion filter requires at least σ^2/h^2 steps to produce the smoothing extent of σ.

To improve the efficiency of the diffusion filter, some authors propose to compute semi-implicit (Drblkov and Mikula, 2008) or implicit numerical (Hale, 2009) solutions of the diffusion equation 5 with several large time steps or a single step. However, these semi-implicit and implicit schemes are often more difficult to implement than the explicit scheme (equation 6) and need to solve large linear systems (Grewenig et al., 2010). In this paper, we use the FED method, proposed by Grewenig et al. (2010) and Weickert et al. (2016), to solve the explicit diffusion (equation 6) with fewer time steps than a conventional explicit method.

Cyclic scheme

The FED method can be considered as a variant of super time stepping schemes that use a set of different time step sizes for the explicit diffusion. As discussed by Grewenig et al. (2010), the FED method is based on two aspects: (1) A Gaussian filter can be approximated by several iterated box filters, and (2) a discrete box filter is equivalent to a cycle of several explicit diffusion steps with varying time step sizes. Therefore, the FED method approximates a diffusion filter with M iterated cycles of n explicit diffusion steps with varying time step sizes.

As discussed by Grewenig et al. (2010) and Weickert et al. (2016), three ($M = 3$) iterated box filters can yield good approximation of a Gaussian filter. In addition, a box filter $B^h_{2n+1}g_i = \sum_{k=-n}^{n}(1/(2n+1))g_k$ is equivalent to a cycle of n explicit diffusions steps: $B^h_{2n+1} = \prod_{i=0}^{n-1}(I+\tau_i\Delta)$ with the varying time step sizes

$$\tau_i = \frac{h^2}{4\cos^2\left(\pi\frac{2i+1}{4n+2}\right)} \tag{7}$$

and the corresponding stopping diffusion time

$$t_n = \sum_{i=0}^{n-1}\tau_i = \frac{h^2}{6}(n^2+n). \tag{8}$$

To explain how this cyclic scheme improves the efficiency of a diffusion filter, let us consider approximating a Gaussian filter with half-width $\sigma^2 = 72h^2$, which corresponds to a diffusion time of $T = (1/2)\sigma^2 = 36h^2$. The conventional explicit scheme requires at least 72 diffusion steps with a constant time step size $\tau = h^2/2$. Using the cyclic scheme with three cycles ($M = 3$), we need to implement each cycle of explicit diffusion with a diffusion time $(1/3)T = 12h^2$. According to equation 8, the diffusion time in each cycle is given by $(h^2/6)(n^2+n)$. This means that $n = 8$ diffusion steps are required to reach the time $12h^2$ in each cycle. Therefore, the cyclic scheme with three cycles requires only $3 \cdot 8 = 24$ explicit diffusion steps to approximate the Gaussian filter ($\sigma^2 = 72h^2$), compared with at least 72 steps for a conventional explicit scheme, which significantly improves the efficiency of the explicit diffusion.

Although the FED method is derived from the 1D linear homogeneous diffusion filter (equation 5), it is actually a general paradigm that is applicable to multidimensional, nonlinear, and anisotropic diffusion filters (Grewenig et al., 2010). Then, we will discuss how to use this efficient FED method in 2D and 3D nonlinear and anisotropic diffusion to simultaneously enhance seismic reflections, faults, and channels.

Enhancing seismic reflections, faults, and channels

Using a diffusion filter to enhance anisotropic (linear in two dimensions and planar in three dimensions) reflections in a seismic image, we expect the diffusion to be anisotropic and aligned in directions along the seismic reflections. As discussed by Fehmers and Höcker (2003) and Hale (2009), such anisotropic diffusion can be designed by steering the diffusion with a diffusion tensor $\mathbf{D}$:

$$\frac{\partial g(\mathbf{x};t)}{\partial t} = \nabla\cdot\mathbf{D}(\mathbf{x})\nabla g(\mathbf{x};t), \tag{9}$$

where $\mathbf{x}$ represents the 2D or 3D spatial coordinates, ∇ is the gradient operator, and the diffusion tensor field $\mathbf{D}(\mathbf{x})$ can be constructed from eigenvectors of seismic structure tensors.

Diffusion with reflection enhancement

As discussed previously in this paper, the eigenvector $\mathbf{u}$ corresponding to the maximum eigenvalue of a structure tensor (equations 2 and 4) is perpendicular to seismic reflections, whereas the other eigenvectors $\mathbf{v}$ and $\mathbf{w}$ are aligned with seismic reflections. Therefore, to enhance seismic reflections, we should smooth the seismic image in directions of $\mathbf{v}$ in two dimensions or $\mathbf{v}$ and $\mathbf{w}$ in three dimensions, but we avoid smoothing in the direction along $\mathbf{u}$. To steer the diffusion in directions along $\mathbf{v}$ and $\mathbf{w}$ for seismic reflection enhancing, we can construct the diffusion tensor $\mathbf{D}(\mathbf{x})$ as

$$\mathbf{D}(\mathbf{x}) = \mu_v(\mathbf{x})\mathbf{v}(\mathbf{x})\mathbf{v}^{\mathsf{T}}(\mathbf{x}) + \mu_w(\mathbf{x})\mathbf{w}(\mathbf{x})\mathbf{w}^{\mathsf{T}}(\mathbf{x}), \quad (10)$$

where the weights $0 \le \mu_v(\mathbf{x}) \le 1$ and $0 \le \mu_w(\mathbf{x}) \le 1$ are used to design a diffusion filter with spatially variant smoothing extents. In most cases, we can set $\mu_v(\mathbf{x}) = \mu_w(\mathbf{x}) = 1$, which yields a spatially invariant and isotropic smoothing extent in the directions along vectors $\mathbf{v}$ and $\mathbf{w}$. In 2D cases, a diffusion tensor field for reflection enhancing can be constructed with only the eigenvector $\mathbf{v}$:

$$\mathbf{D}(\mathbf{x}) = \mu_v(\mathbf{x})\mathbf{v}(\mathbf{x})\mathbf{v}^{\mathsf{T}}(\mathbf{x}). \quad (11)$$

The multidimensional and anisotropic diffusion (equation 9) can also be solved explicitly in k diffusion steps:

$$g(\mathbf{x}_i; t_{k+1}) = (I + \tau\nabla \cdot \mathbf{D}(\mathbf{x}_i)\nabla)g(\mathbf{x}_i; t_k)) \quad (12)$$

with an initial image $g(\mathbf{x}; t_0) = g(\mathbf{x})$ and a constant time step size τ. To speed up the diffusion process, we can also use the FED method with M cycles of n explicit diffusion steps. In all examples in this paper, we use $M = 3$ for the number of FED cycles. We use equation 8 to compute the smallest number of steps n in one cycle such that the stopping time $t_n \approx T/M$. For step i in each cycle, we compute the time step size τ_i using equation 7. The FED method for anisotropic diffusion with reflection enhancing can be described as in the following pseudocodes in Algorithm 1.

Figure 4 shows a 2D example of using anisotropic diffusion to enhance seismic reflections. In this example, we set the stopping time $T = 32$ and $M = 3$, which yields 24 explicit diffusion steps to compute the smoothed seismic image shown in Figure 4a. With an eight-core computer, computing the smoothed image in Figure 4a takes only 0.037 s compared to 0.086 s in computing the smoothed image in Figure 3a by using the structure-oriented smoothing method (Hale, 2009). In this example, we construct the diffusion tensor field as $\mathbf{D}_r(\mathbf{x}) = \mathbf{v}(\mathbf{x})\mathbf{v}^{\mathsf{T}}(\mathbf{x})$, which yields an anisotropic diffusion with a constant smoothing extent along seismic reflections. We observe that the seismic reflections in the smoothed image (Figure 4a) are cleaner and more continuous compared to the input seismic image (Figure 1a). Most of the noise in the original seismic image (Figure 1a) is removed as shown in the input-output difference image (Figure 4b). However, the faults, recognized as lateral discontinuities in the seismic image, are also smoothed out because of the constant-extent smoothing along seismic reflections.

Diffusion with reflection and fault enhancement

To preserve reflection discontinuities at faults, we should stop the anisotropic diffusion near the faults. This means that we need to construct anisotropic diffusion with spatially variant smoothing extents, which can be designed using diffusion tensors with spatially variant weights as shown in equations 10 and 11. Such spatially variant diffusion is similar to the problem of diffusion with edge preserving (e.g., Alvarez et al., 1992; Weickert, 1997, 2001; Fehmers and Höcker, 2003; Hale, 2009). Hale (2009) first computes an image of faults or edges and then uses the image to stop diffusion across the faults. In this method, the fault image is not updated and therefore the diffusion is linear. Most methods (Alvarez et al., 1992; Weickert, 1997, 2001; Fehmers and Höcker, 2003) construct nonlinear diffusion for preserving edges, which keeps updating the edge image while iteratively performing the diffusion process. Linear diffusion without updating the edge image is often more efficient. Nonlinear diffusion is less efficient, but it can gradually update the edge image

Algorithm 1. Diffusion with reflection enhancement.

1. Input:
2. (a) image $g(\mathbf{x})$;
3. (b) stopping time T;
4. (c) number of FED cycles M ($M = 3$)
5. **Initialization:**
6. (a) initial image $g(\mathbf{x}; 0) = g(\mathbf{x})$;
7. (b) compute the diffusion tensor $\mathbf{D}_r(\mathbf{x}) = \mathbf{v}\mathbf{v}^{\mathsf{T}} + \mathbf{w}\mathbf{w}^{\mathsf{T}}$;
8. (c) compute the smallest n of one cycle such that stopping time $t_n \approx T/M$ (equation 8);
9. (d) compute the time step sizes τ_i (equation 7) in one cycle
10. **Diffusion loop:**
11. **for** $k := 0$ **to** M **step** 1 **do**
12. **for** $i := 0$ **to** n **step** 1 **do**
13. $g(\mathbf{x}; t_{i+1}) = (I + \tau_i\nabla \cdot D_r(\mathbf{x})\nabla)g(\mathbf{x}; t_i))$
14. **end for**
15. $g(\mathbf{x}; t_{k+1}) \leftarrow g(\mathbf{x}; t_n)$
16. **end for**
17. **Output:**
18. (a) smoothed seismic image $g(\mathbf{x}; t_M)$

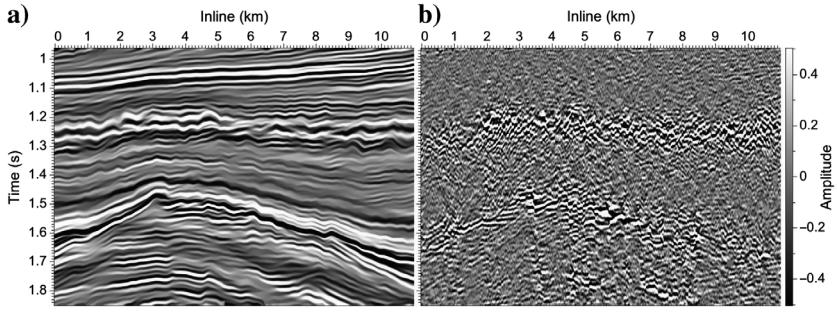

Figure 4. (a) Smoothed image computed by the proposed fast anisotropic diffusion with reflection enhancing (computational time: 0.037 s). (b) Input-output difference.

during the diffusion process. In this paper, we apply nonlinear diffusion to iteratively update the image of seismic faults while smoothing seismic reflections. We also apply approximate fault-oriented smoothing to the fault image to enhance the fault features. This iteratively updated and enhanced fault image is used to preserve discontinuities corresponding to faults in the smoothed seismic image, and it also provides a good detection of faults.

To detect edges in an image, Weickert (2001) uses a scalar-valued diffusivity function defined as

$$w(\mathbf{x}) = \begin{cases} 1, & |\nabla g(\mathbf{x})|^2 = 0 \\ 1 - \exp\left(-\frac{3.315}{(|\nabla g(\mathbf{x})|^2/\alpha^2)^4}\right), & |\nabla g(\mathbf{x})|^2 > 0 \end{cases}, \quad (13)$$

where $g(\mathbf{x})$ is an input image and α is a constant parameter separating low-contrast regions from high-contrast locations where edges may exist (Weickert, 2001). To detect faults from seismic reflections, we cannot directly use the image gradient to compute a diffusivity function because the large gradients of a seismic image do not correspond to faults.

To detect the faults that are recognized as lateral discontinuities of seismic reflections, we should use directional derivatives of the seismic image to compute structure-oriented diffusivity function:

$$s(\mathbf{x}) = \begin{cases} 1, & d^2(\mathbf{x}) = 0 \\ 1 - \exp\left(-\frac{3.315}{(d^2(\mathbf{x})/\alpha^2)^4}\right), & d^2(\mathbf{x}) > 0 \end{cases}, \quad (14)$$

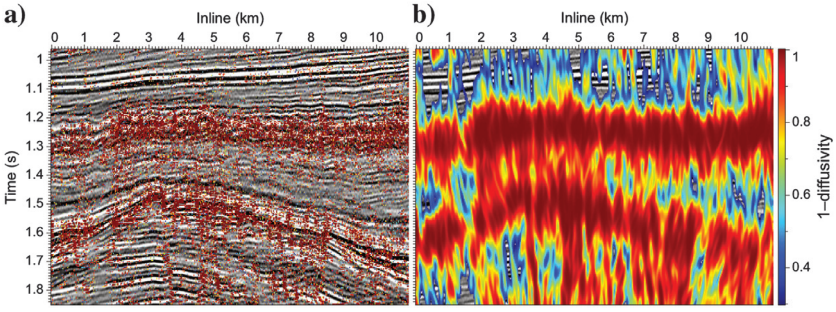

Figure 5. Diffusivity image (a) before and (b) after anisotropic diffusion in the directions along eigenvectors $\mathbf{u}$ (perpendicular to the reflections).

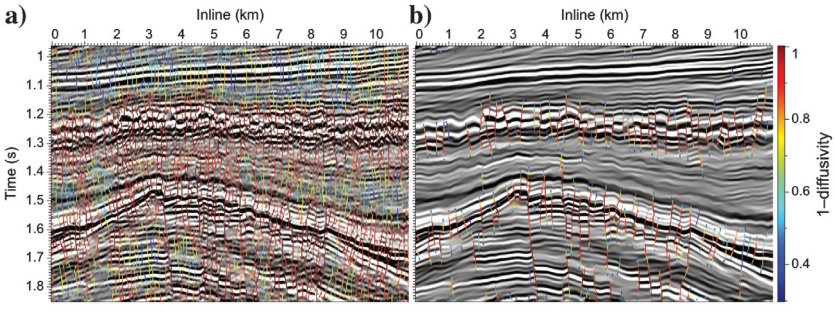

Figure 6. (a) Thinned diffusivity image computed from Figure 5b by keeping its nonzero values only on the ridges. (b) Thinned diffusivity image after the anisotropic diffusion with reflection and fault enhancing.

where $d(\mathbf{x})$ is defined as $d(\mathbf{x}) = \mathbf{v}^{\mathsf{T}}(\mathbf{x})\nabla g(\mathbf{x}) + \mathbf{w}^{\mathsf{T}}(\mathbf{x})\nabla g(\mathbf{x})$. The functions $\mathbf{v}^{\mathsf{T}}(\mathbf{x})\nabla g(\mathbf{x})$ and $\mathbf{w}^{\mathsf{T}}(\mathbf{x})\nabla g(\mathbf{x})$ represent the directional derivatives of the seismic image $g(\mathbf{x})$ in the directions along eigenvectors $\mathbf{v}(\mathbf{x})$ and $\mathbf{w}(\mathbf{x})$, respectively. Because the eigenvectors $\mathbf{v}(\mathbf{x})$ and $\mathbf{w}(\mathbf{x})$ are aligned within the seismic reflections, the directional derivatives are computed along the seismic reflections. In 2D cases, the directional derivatives are computed only along the eigenvectors $\mathbf{v}(\mathbf{x})$: $d(\mathbf{x}) = \mathbf{v}^{\mathsf{T}}(\mathbf{x})\nabla g(\mathbf{x})$. Of course, there are a lot more sophisticated seismic attributes including semblance (Marfurt et al., 1998), coherency (Marfurt et al., 1999), variance (Van Bemmel and Pepper, 2000; Randen et al., 2001),and fault likelihoods (Hale, 2013) that may be even better than the structure-oriented diffusivity to detect faults from an original noisy seismic image. However, as denoted in equation 14, computing the diffusivity is much more efficient than all of these sophisticated attributes, and we will show that the diffusivity will be gradually updated and enhanced during our iterative diffusion and eventually provide a good detection of faults.

Figure 5a shows a fault image $f(\mathbf{x}) = 1 - s(\mathbf{x})$, where $s(\mathbf{x})$ is diffusivity computed using equation 14 with $\alpha = 0.12$. In this image, the features with relatively high values detect the fault positions in the seismic image but also highlight noise, which does not correspond to faults. In addition, the fault features are discontinuous as shown in this image (Figure 5). Therefore, we might want to further smooth the fault image along fault orientations so that the fault features are enhanced and more continuous while the features unrelated to faults are suppressed.

As discussed by Bakker (2002) and Hale (2009), faults often cut through multiple reflections and are often approximately dipping in directions perpendicular to seismic reflections. Therefore, the eigenvectors $\mathbf{u}(\mathbf{x})$ can be good approximations of the fault dip directions in most cases. Also as shown by Wu (2017), the fault strike directions can be approximated by eigenvectors $\mathbf{w}(\mathbf{x})$. Therefore, we may want to smooth the diffusivity or fault image (Figure 5) in directions of eigenvectors $\mathbf{u}(\mathbf{x})$ and $\mathbf{w}(\mathbf{x})$ to enhance the image features related to faults and suppress noise that is often arbitrarily oriented. To smooth the image along the eigenvectors $\mathbf{u}(\mathbf{x})$ and $\mathbf{w}(\mathbf{x})$, we use the anisotropic diffusion described in Algorithm 1 with the diffusion tensor field constructed as $\mathbf{D}_{uw}(\mathbf{x}) = \mathbf{u}(\mathbf{x})\mathbf{u}^{\mathsf{T}}(\mathbf{x}) + \mathbf{w}(\mathbf{x})\mathbf{w}^{\mathsf{T}}(\mathbf{x})$. In 2D cases, we smooth the fault image (Figure 5) along the eigenvectors $\mathbf{u}(\mathbf{x})$ with the diffusion tensor constructed as $\mathbf{D}(\mathbf{x}) = \mathbf{u}(\mathbf{x})\mathbf{u}^{\mathsf{T}}(\mathbf{x})$. Figure 5a shows smoothed fault image $f_u(\mathbf{x}) = 1 - s_u(\mathbf{x})$, where $s_u(\mathbf{x}) = \langle s(\mathbf{x})\rangle_u$ and the angle brackets $\langle\cdot\rangle_u$ represent the

anisotropic diffusion in directions along eigenvectors $\mathbf{u}(\mathbf{x})$. The fault features in this image (Figure 5b) are more continuous compared with the one (Figure 5a) before the smoothing. However, we do not expect faults to be as thick as the features apparent in this image (Figure 5b). Therefore, we keep only the values on the ridges of the image and we set the values elsewhere to be zero to compute the corresponding thinned image as shown in Figure 6a. In this thinned image (Figure 6a), nonzero values are apparent at samples that are on faults but also at samples unrelated to faults. However, this is just an initial map of faults used to stop smoothing at faults in the nonlinear diffusion process. This map will be iteratively updated and improved during the iterative anisotropic diffusion process.

The nonlinear and anisotropic diffusion for enhancing seismic reflections and updating the fault map can be described as in the pseudocodes in Algorithm 2.

In this algorithm of anisotropic diffusion with fault enhancing, we do not update the diffusion tensor field at each diffusion step i; instead, we only update it at each cycle k: $\mathbf{D}_f(\mathbf{x};t_k) = s_t(\mathbf{x};t_k)\mathbf{v}\mathbf{v}^\top + s_t(\mathbf{x};t_k)\mathbf{w}\mathbf{w}^\top$, where only the thinned and smoothed diffusivity $s_t(\mathbf{x};t_k)$ is updated at each cycle but the vectors $\mathbf{v}$ and $\mathbf{w}$ are not updated. This means that the diffusivity and diffusion tensor field are computed only M ($M = 3$ in this paper) times during the whole diffusion process. In 2D cases, the diffusion tensor field is computed using only the eigenvectors $\mathbf{v}(\mathbf{x})$: $\mathbf{D}_f(\mathbf{x};t_k) = s_t(\mathbf{x};t_k)\mathbf{v}\mathbf{v}^\top$. Using this method, we are able to simultaneously obtain a smoothed seismic image with fault preservation and an enhanced fault image that highlights fault locations.

Figure 6b shows the finally updated fault image $f_t(x) = 1 - s_t(\mathbf{x};t_k)$ overlaid with the finally updated seismic image. We observe that a lot of suspicious features in the initial fault image (Figure 6a) are removed in the updated fault image (Figure 6b). The nonzero samples in the initial fault image (Figure 6a) indicate that the left- and right-neighboring reflections of these samples are discontinuous. However, such reflection discontinuities do not necessarily correspond to faults and they may actually correspond to noise. During the nonlinear and anisotropic diffusion process (Algorithm 2), smoothing is performed along the left and right reflections of these nonzero samples, but it is stopped at these samples. After some diffusion steps, the noise on the left and right reflections of these nonzero samples will be smoothed out. The smoothed reflections on the left and right sides of these nonzero samples will become consistent and continuous if these samples do not correspond to faults, but the left and right reflections will be still discontinuous and inconsistent if these samples correspond to true faults. Therefore, in the updated fault image (Figure 6b), the nonzero values corresponding to noise are removed whereas those corresponding to true faults are preserved. This updated fault image provides a good detection of the fault positions.

Algorithm 2. Anisotropic diffusion with reflection and fault enhancement.

1. **Input:**
2. (a) image $g(\mathbf{x})$;
3. (b) stopping time T;
4. (c) number of FED cycles M ($M = 3$)
5. **Initialization:**
6. (a) initial image $g(\mathbf{x};0) = g(\mathbf{x})$;
7. (b) compute the diffusion tensor $\mathbf{D}_{uw}(\mathbf{x}) = \mathbf{u}\mathbf{u}^\top + \mathbf{w}\mathbf{w}^\top$ for diffusivity smoothing;
8. (c) compute the smallest n of one cycle such that stopping time $t_n \approx T/M$ (equation 8);
9. (d) compute the time step sizes τ_i (equation 7) in one cycle
10. **Diffusion loop:**
11. **for** $k := 0$ to M **step 1 do**
12. compute the diffusivity $s(\mathbf{x};t_k)$ from $g(\mathbf{x};t_k)$;
13. compute the smoothed diffusivity $s_{uw}(\mathbf{x};t_k) = \langle s(\mathbf{x};t_k)\rangle_{uw}$;
14. compute the thinned diffusivity $s_t(\mathbf{x};t_k)$ from $s_{uw}(\mathbf{x};t_k)$;
15. compute the diffusion tensor: $\mathbf{D}_f(\mathbf{x};t_k) = s_t(\mathbf{x};t_k)\mathbf{v}\mathbf{v}^\top + s_t(\mathbf{x};t_k)\mathbf{w}\mathbf{w}^\top$;
16. **for** $i := 0$ **to** n **step** 1**do**
17. $g(\mathbf{x};t_{i+1}) = (I + \tau_i \nabla \cdot D_f(\mathbf{x};t_k)\nabla)g(\mathbf{x};t_i))$
18. **end for**
19. $g(\mathbf{x};t_{k+1}) \leftarrow g(\mathbf{x};t_n)$
20. **end for**
21. **Output:**
22. (a) smoothed seismic image $g(\mathbf{x};t_M)$ with fault preservation;
23. (b) enhanced fault image $f_t(x) = 1 - s_t(\mathbf{x};t_M)$

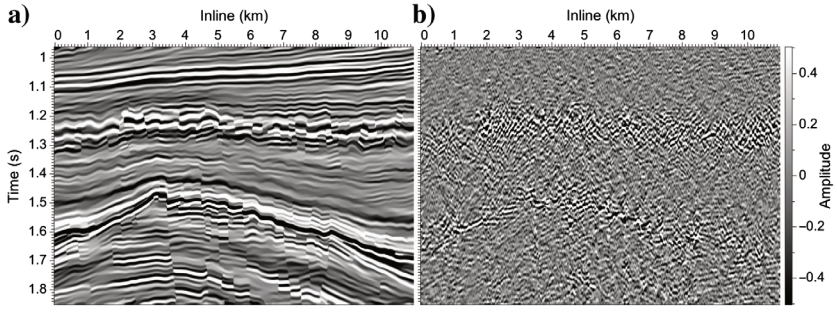

Figure 7. (a) Smoothed image computed by the proposed anisotropic diffusion with reflection and fault enhancing. (b) Input-output difference.

Figure 7a and 7b shows the smoothed seismic image and the input-output difference image, respectively. We observe that the noise in the seismic image is removed. The seismic reflections are continuous everywhere but are discontinuous at faults. The seismic reflections and faults in this smoothed image (Figure 7a) are clearer than those in the original seismic image (Figure 1a). Although this method is applied only to a 2D example in this paper, the corresponding algorithm (Algorithm 2) is actually designed in three dimensions, and therefore it is applicable to a 3D seismic image to simultaneously detect 3D faults and enhance reflections and faults in the image.

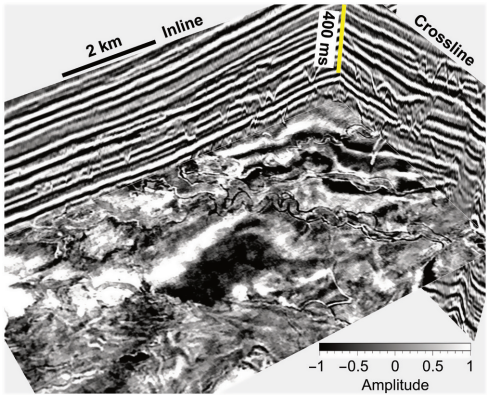

Figure 8. A 3D seismic image with channels apparent on the time slice.

Diffusion with reflection and channel enhancement

In addition to the structural features of reflections and faults, stratigraphic features such as channels are also contained in a seismic image, as shown in Figure 8. This 3D seismic image is a subset extracted from the 1520 km^2 Parihaka 3D seismic survey located at the Taranaki Basin, a broad sedimentary basin on the western side of the North Island, New Zealand. This Taranaki Basin covers approximately 100,000 km^2, and the basin lying offshore is mostly at water depths between 50 and 250 m. A lot of large-scale and fine-scale channels are apparent within the acquired Parihaka 3D seismic volume (Johnston, 2014), and some of the channels are obviously visible on the time slice of the subset volume (Figure 8). Seismic channels are often aligned within dipping seismic reflections. We are able to observe channels in the horizontal time slice of the 3D seismic image in Figure 8 because the reflections in this seismic image are only slightly dipping.

Similar to seismic faults, the channels are also recognized as lateral discontinuities along seismic reflections as shown in the vertical slices in the 3D seismic image (Figure 8). Therefore, if we apply the structure-oriented smoothing method (Hale, 2009) to smooth the seismic image along seismic reflections, we are able to enhance the reflections but also smooth out the channels as shown in Figure 9. Similarly, if we perform simple anisotropic diffusion (Algorithm 1) along seismic reflections, we obtain almost the same smoothed results as shown in Figure 10. Figure 10a and 10b, respectively, shows the smoothed image and input-output difference image computed using the anisotropic diffusion (Algorithm 1) with a diffusion tensor field $\mathbf{D}(\mathbf{x})$ defined as $\mathbf{D}(\mathbf{x}) = \mathbf{v}\mathbf{v}^{\mathsf{T}} + \mathbf{w}\mathbf{w}^{\mathsf{T}}$. In Figure 10a and 10b, we observe that noise is removed and reflections are more continuous as shown in the vertical slices but the channels are also removed as shown in the horizontal time slices. Note that the fast explicit anisotropic diffusion used in this paper requires only 24.9 s to compute the smoothed image in Figure 10a compared with 43.8 s to compute the smoothed image in Figure 9a by using Hale's method, which, again, demonstrates that the FED method is much more efficient.

Because the eigenvectors $\mathbf{v}(\mathbf{x})$ are laterally perpendicular to seismic channels whereas the eigenvectors $\mathbf{w}(\mathbf{x})$ are

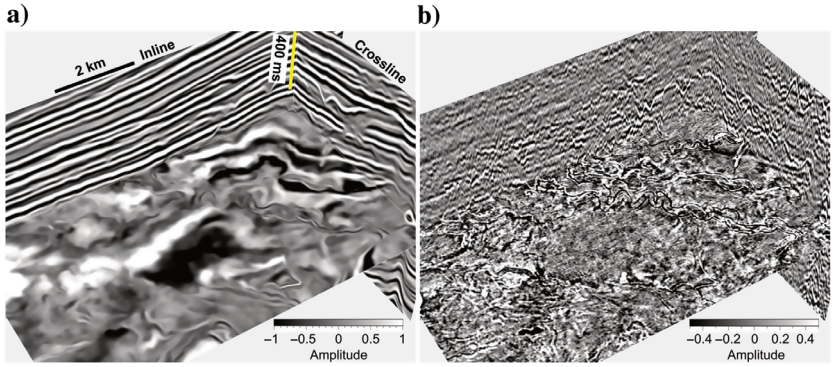

Figure 9. (a) Smoothed image computed by Hale's method (computational time: 43.8 s). (b) Input-output difference.

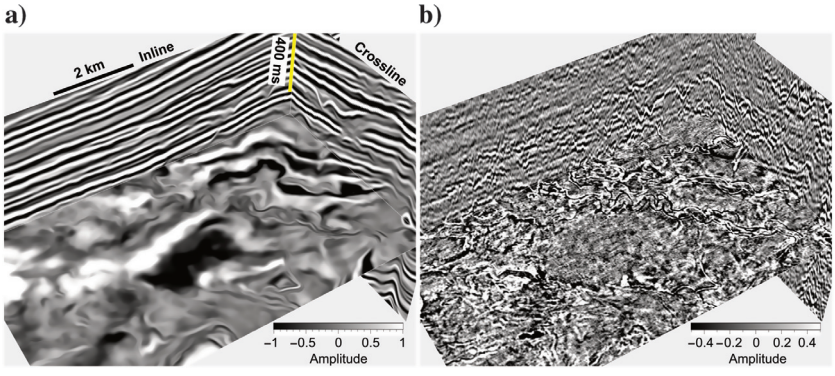

Figure 10. (a) Smoothed image computed by the proposed fast anisotropic diffusion with reflection enhancing (computational time: 24.9 s). (b) Input-output difference.

laterally parallel to the channels (Figure 2), we may define the diffusion tensor field as $\mathbf{D}(\mathbf{x})=\mathbf{w}\mathbf{w}^{\top}$ to smooth the seismic image only in directions along eigenvectors $\mathbf{w}(\mathbf{x})$ to enhance seismic channels. Figure 11a and 11b, respectively, shows the smoothed image and input-output difference image computed using the anisotropic diffusion (Algorithm 1) with a diffusion tensor field $\mathbf{D}(\mathbf{x})$ defined as $\mathbf{D}(\mathbf{x})=\mathbf{w}\mathbf{w}^{\top}$. In Figure 11a and 11b, we observe that noise is removed to some extent and reflections and channels are enhanced as shown in the vertical and horizontal slices.

However, some noises, especially those in the crossline slice, are not removed because we smooth the image along only one direction of the eigenvector $\mathbf{w}(\mathbf{x})$ and the noises may be coherent in this direction. Moreover, the smoothing generates some suspicious linear features in the areas highlighted by the yellow ellipses (Figure 11a), whereas the image features in the same areas of the original image (Figure 8) are actually isotropic. By smoothing along reflections in only one direction of $\mathbf{w}(\mathbf{x})$, we actually assume that linear features, such as channels, are apparent everywhere along seismic reflections in the seismic image. This assumption is not true in most cases in which the image features along seismic reflections are mostly isotropic and are linear (anisotropic) in only limited areas. This means that the anisotropy of image features along reflections is actually spatially variant, which indicates that we should also apply spatially variant anisotropic smoothing to enhance the image features, instead of applying smoothing along eigenvectors $\mathbf{w}(\mathbf{x})$ everywhere in the seismic image.

Specifically, in areas with isotropic features along reflections, we should apply isotropic smoothing along reflections in the directions of eigenvectors $\mathbf{v}(\mathbf{x})$ and $\mathbf{w}(\mathbf{x})$. In areas with anisotropic (linear) features along reflections, we should apply anisotropic smoothing along reflections only in the direction of eigenvector $\mathbf{w}(\mathbf{x})$, which is aligned with the linear features. To implement such spatially variant (along reflections) smoothing, we use anisotropic diffusion with a diffusion tensor field defined as follows:

$$\mathbf{D}(\mathbf{x})=c(\mathbf{x})\mathbf{v}(\mathbf{x})\mathbf{v}^{\top}(\mathbf{x})+\mathbf{w}(\mathbf{x})\mathbf{w}^{\top}(\mathbf{x}), \tag{15}$$

where $0\le c(\mathbf{x})\le 1$ is a map that highlights seismic channels with relatively low values. Near seismic channels, $c(\mathbf{x})$ is close to zero and the smoothing in the direction of $\mathbf{v}(\mathbf{x})$ (perpendicular to channels) will be stopped. In areas without channels, $c(\mathbf{x})$ is close to one and the smoothing will be isotropic along reflections in the direction of $\mathbf{v}(\mathbf{x})$ and $\mathbf{w}(\mathbf{x})$.

We compute such a map ($c(\mathbf{x})$) of seismic channels, again, from the structure-oriented diffusivity $s(\mathbf{x})$ (equation 14). Figure 12a shows a structure-oriented diffusivity image computed from the original 3D seismic image (Figure 8) with $\alpha=0.1$. This diffusivity image highlights (with relatively low values) channels and also noise in the

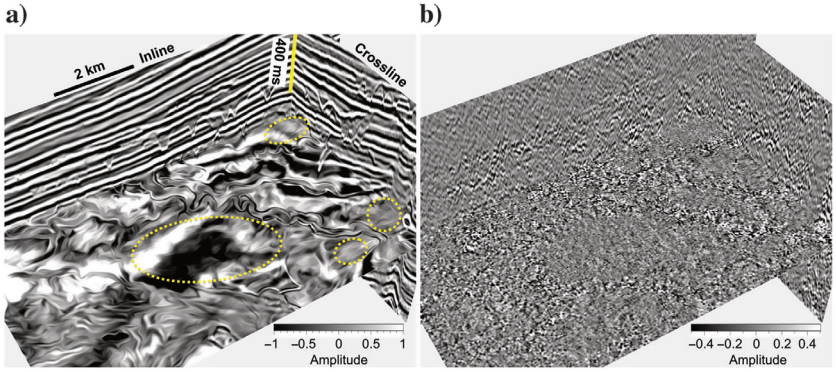

Figure 11. (a) Smoothed image by the proposed anisotropic diffusion with channel enhancing. (b) Input-output difference.

Algorithm 3. Anisotropic diffusion with reflection and channel enhancement.

1. **Input:**
2. (a) image $g(\mathbf{x})$;
3. (b) stopping time T;
4. (c) number of FED cycles M ($M=3$)
5. **Initialization:**
6. (a) initial image $g(\mathbf{x};0)=g(\mathbf{x})$;
7. (b) compute the diffusion tensor $\mathbf{D}_w(\mathbf{x})=\mathbf{w}\mathbf{w}^{\top}$ for diffusivity smoothing;
8. (c) compute the smallest n of one cycle such that stopping time $t_n\approx T/M$ (equation 8);
9. (d) compute the time step sizes τ_i (equation 7) in one cycle
10. **Diffusion loop:**
11. **for** $k:=0$ **to** M **step** 1**do**
12. compute the diffusivity $s(\mathbf{x};t_k)$ from $g(\mathbf{x};t_k)$;
13. compute the smoothed diffusivity $s_w(\mathbf{x};t_k)=\langle s(\mathbf{x};t_k)\rangle_w$;
14. compute the diffusion tensor: $\mathbf{D}_c(\mathbf{x};t_k)=s_w(\mathbf{x};t_k)\mathbf{v}\mathbf{v}^{\top}+\mathbf{w}\mathbf{w}^{\top}$;
15. **for** $i:=0$ **to** n **step** 1**do**
16. $g(\mathbf{x};t_{i+1})=(I+\tau_i\nabla\cdot D_c(\mathbf{x};t_k)\nabla)g(\mathbf{x};t_i))$
17. **end for**
18. $g(\mathbf{x};t_{k+1})\leftarrow g(\mathbf{x};t_n)$
19. **end for**
20. **Output:**
21. (a) smoothed seismic image $g(\mathbf{x};t_M)$ with fault preservation;
22. (b) enhanced channel image $c(\mathbf{x})=s_w(\mathbf{x};t_M)$

3D seismic image. Similar to the diffusivity used in Algorithm 1, this diffusivity image is just an initial map of channels used to construct the diffusion tensor field. During the diffusion process, we will iteratively update the map and also enhance the map by smoothing it along channel orientations ($\mathbf{w}(\mathbf{x})$) in each update. The pseudocodes below (Algorithm 3) describe the diffusion scheme that we used to simultaneously compute an image of channels and enhance seismic reflections and channels.

In the whole diffusion process, we totally update the diffusivity image $s(\mathbf{x};t_k)$ M times ($M=3$ in this paper). For each update, we smooth the diffusivity image $s(\mathbf{x};t_k)$ in the direction of $\mathbf{w}(\mathbf{x})$ to enhance the image features corresponding to seismic channels. This smoothed diffusivity image $s_w(\mathbf{x};t_k)=\langle s(\mathbf{x};t_k)\rangle_w$ is further used to update the diffusion tensor field $\mathbf{D}_c(\mathbf{x};t_k)=s_w(\mathbf{x};t_k)\mathbf{v}\mathbf{v}^\top+\mathbf{w}\mathbf{w}^\top$. This finally updated and smoothed diffusivity image $s_w(\mathbf{x};t_M)$ is also an output as a map detecting seismic channels.

Figure 12b shows the final output diffusivity image in which the noise is removed and the channel features are much clearer and continuous compared to the initial diffusivity image (Figure 12a). Figure 13a shows the smoothed seismic image $g(\mathbf{x};t_M)$, in which the seismic reflections and channels are enhanced. In addition, the suspicious linear features, highlighted by the yellow ellipses in Figure 11a, do not appear in this smoothed seismic image (Figure 13a). From the input-output difference image shown in Figure 13b, noise in the original seismic image is removed but the seismic channels are well-preserved.

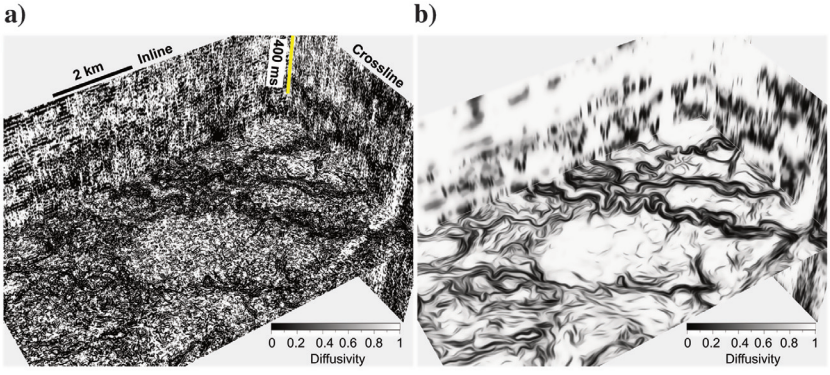

Figure 12. A diffusivity image (a) before and (b) after the anisotropic diffusion with reflection and channel enhancing.

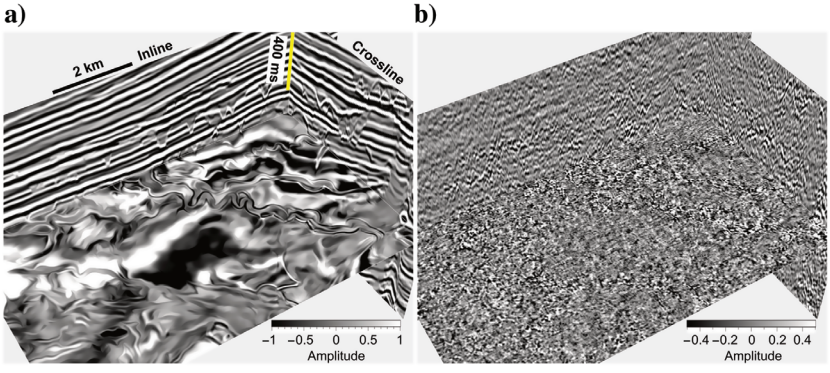

Figure 13. (a) Smoothed image by the proposed anisotropic diffusion with reflection and channel enhancing. (b) Input-output difference.

Methods	Diffusion tensors	Smoothing directions of V and W	Smoothing extents
Method one	$\mathbf{v}\mathbf{v}^\top+\mathbf{w}\mathbf{w}^\top$	Isotropic	Spatially constant
Method two	$s_t(\mathbf{x};t_k)(\mathbf{v}\mathbf{v}^\top+\mathbf{w}\mathbf{w}^\top)$	Isotropic	Spatially variant
Method three	$s_w(\mathbf{x};t_k)\mathbf{v}\mathbf{v}^\top+\mathbf{w}\mathbf{w}^\top$	Anisotropic	Spatially variant

Figure 14. A comparison of diffusion tensors in all the three smoothing methods. These tensors define the smoothing directions and extents.

Discussions

In this paper, we first discussed a general method of enhancing seismic reflections, which, however, blurs faults and channels in the seismic image. We then discussed a method to simultaneously enhance reflections and faults in a seismic image while computing an image of seismic faults. We finally discussed a similar method to simultaneously enhance reflections and channels in a seismic image while computing an image of channels. We implement all the methods using the same FED scheme but with different diffusion tensor fields, which define the smoothing orientations and smoothing extents for the diffusion process.

As shown in Figure 14, the diffusion tensors for the three methods, respectively, are defined as (1) $\mathbf{D}_r(\mathbf{x})=\mathbf{v}\mathbf{v}^\top+\mathbf{w}\mathbf{w}^\top$, (2) $\mathbf{D}_f(\mathbf{x};t_k)=s_t(\mathbf{x};t_k)(\mathbf{v}\mathbf{v}^\top+\mathbf{w}\mathbf{w}^\top)$, and (3) $\mathbf{D}_c(\mathbf{x};t_k)=s_w(\mathbf{x};t_k)\mathbf{v}\mathbf{v}^\top+\mathbf{w}\mathbf{w}^\top$. As discussed in the previous sections, $s_t(\mathbf{x};t_k)$ represents a thinned fault image or mapping and $s_w(\mathbf{x};t_k)$ represents an image of seismic channels. From the definitions, the smoothing extents in the first method are spatially constant in the directions of $\mathbf{v}$ and $\mathbf{w}$ because the weights for the two terms $\mathbf{v}\mathbf{v}^\top$ and $\mathbf{w}\mathbf{w}^\top$ are equal to one. In the second method, the smoothing extents in the directions of $\mathbf{v}$ and $\mathbf{w}$ are spatially variant and are defined by a weighting map $s_t(\mathbf{x};t_k)$. In the second method, the smoothing extents in the direction of $\mathbf{v}$ are spatially variant and are defined by a weighting map $s_w(\mathbf{x};t_k)$, whereas the smoothing extents in the direction of $\mathbf{w}$ are spatially constant.

If we consider the smoothing in three directions of eigenvectors $\mathbf{u}(\mathbf{x})$, $\mathbf{v}(\mathbf{x})$, and $\mathbf{w}(\mathbf{x})$, then the diffusion in all the methods is anisotropic because in these methods we smooth a seismic image in directions parallel ($\mathbf{u}(\mathbf{x})$ and $\mathbf{v}(\mathbf{x})$) to but not perpendicular ($\mathbf{u}(\mathbf{x})$) to the reflections. However, because the direction of eigenvector $\mathbf{u}(\mathbf{x})$ is not used in constructing the diffusion tensors in all three methods, we can actually consider the smoothing in only two directions of eigenvectors $\mathbf{v}(\mathbf{x})$ and $\mathbf{w}(\mathbf{x})$ & *thinsp*;. Then, the smoothing in the first and second methods is always isotropic because the smoothing extents ($s_t(\mathbf{x};t_k)$) in the directions of $\mathbf{v}(\mathbf{x})$ and $\mathbf{w}(\mathbf{x})$ are always the same at each image sample $\mathbf{x}$. The smoothing in the third method is mostly anisotropic ($s_w(\mathbf{x};t_k) < 1$ in most areas) and is isotropic only in areas with $s_w(\mathbf{x};t_k) = 1$.

For seismic images with faults and channels, it is convenient to construct an anisotropic diffusion filter to simultaneously enhance reflections, faults, and channels by defining the diffusion tensor as $s_t(\mathbf{x};t_k)[s_w(\mathbf{x};t_k)\mathbf{v}\mathbf{v}^\top + \mathbf{w}\mathbf{w}^\top]$, where, again, the mappings $s_t(\mathbf{x};t_k)$ and $s_w(\mathbf{x};t_k)$ highlight faults and channels with relatively low values. In this case, the diffusion will be anisotropic and the smoothing extent will be spatially variant.

Conclusion

We have discussed structure- and stratigraphy-oriented smoothing methods to simultaneously enhance reflections, faults, and channels in a seismic image while computing images of faults and channels. We implement these methods using FED with different diffusion tensors, which control the smoothing orientations and extents in the diffusion. In constructing such diffusion tensors, we use seismic structural and stratigraphic orientations to define the diffusion orientations and we use mappings of faults and channels to define the diffusion extents. During the entire diffusion processing, the mappings of faults and channels are iteratively updated together with the seismic image. In addition, these mappings are further enhanced at each update by fault- or channel-oriented smoothing.

Mappings with fault and channel detections are required to define small diffusion extents near the faults and channels and therefore to preserve reflection discontinuities near the faults and channels when smoothing a seismic image. On the other hand, the fault and channel mappings, computed as measurements of reflection discontinuities, are often sensitive to noise, which also generates reflection discontinuities in the seismic image. The smoothing of the seismic image can be helpful to remove the suspicious fault and channel detections due to noise. This is why we simultaneously update the fault and channel mappings while smoothing the seismic image. In addition, the reflection discontinuities corresponding to noise are often spatially inconsistent while faults and channels are apparent as spatially coherent reflection discontinuities in a seismic image. Therefore, before using the fault and channel mappings to construct diffusion tensors, we first apply fault- or channel-oriented smoothing to further enhance faults and channels and suppress noise in the mappings. In fault-oriented smoothing, we use the eigenvectors $\mathbf{u}$ and $\mathbf{w}$ to approximate the fault dip and strike directions, respectively. This has been proven to be a good approximation in many cases, but can be poor for some cases in which the faults are not dipping in directions perpendicular to seismic reflections. Therefore, a better way of estimating fault orientations is still desirable to further improve the methods discussed in this paper.

The cyclic scheme of the FED method helps to reduce the extra computational costs required in updating and enhancing the fault and channel images. First, this scheme speeds up the diffusion processing by significantly reducing the number of diffusion steps. Second, in this scheme we do not update the fault and channel images at each diffusion step, we actually update these images only at each cycle and in total only three times in the entire smoothing processing.

Although faults and channels can be recognized as lateral reflection discontinuities in a seismic image, channels are also consistent linear features aligned within reflections in a 3D seismic image. Therefore, to enhance channels in a 3D seismic image, we not only sharpen the reflection discontinuities at the channel boundaries, but we also smooth the seismic image along the stratigraphic orientations to enhance the linear channel features.

Acknowledgments

This work greatly benefited from discussions with S. Fomel. The 2D seismic image with faults is a subsection extracted from the F3 seismic data, which is available on the website: https://opendtect.org/osr/pmwiki.php/Main/NetherlandsOffshoreF3BlockComplete4GB. The 3D seismic image with channels is a subset of the Parihaka 3D data set, which is provided by New Zealand Crown Minerals through the SEG Wiki website (http://wiki.seg.org/wiki/Parihaka-3D). This research is supported by the sponsors of the Texas Consortium for Computational Seismology.

Data and materials availability

Data associated with this research are available and can be accessed via the following URL: Note: A digital object identifier (DOI) linking to the data in a general or discipline-specific data repository is strongly preferred.

References

AlBinHassan, N. M., Y. Luo, and M. N. Al-Faraj, 2006, 3D edge-preserving smoothing and applications: Geophysics, **71**, no. 4, P5–P11, doi: 10.1190/1.2213050.

Alvarez, L., P.-L. Lions, and J.-M. Morel, 1992, Image selective smoothing and edge detection by nonlinear diffusion. II: SIAM Journal on Numerical Analysis, **29**, 845–866, doi: 10.1137/0729052.

Arias, E., 2016, Estimating seismic reflection slopes: Master's thesis, Colorado School of Mines.

Bakker, P., 2002, Image structure analysis for seismic interpretation: Ph.D. thesis, Delft University of Technology.

Bakker, P., L. J. van Vliet, and P. W. Verbeek, 1999, Edge preserving orientation adaptive filtering: Proceedings of the IEEE Computer Society Conference on Computer Vision and Pattern Recognition.

Chopra, S., and K. Marfurt, 2007, Seismic attributes for prospect identification and reservoir characterization: SEG and EAGE.

Drblkov, O., and K. Mikula, 2008, Convergence analysis of finite volume scheme for nonlinear tensor anisotropic diffusion in image processing: SIAM Journal on Numerical Analysis, **46**, 37–60, doi: 10.1137/070685038.

Fehmers, G. C., and C. F. Höcker, 2003, Fast structural interpretation with structure-oriented filtering: Geophysics, **68**, 1286–1293, doi: 10.1190/1.1598121.

Fomel, S., 2002, Applications of plane-wave destruction filters: Geophysics, **67**, 1946–1960, doi: 10.1190/1.1527095.

Gersztenkorn, A., and K. J. Marfurt, 1999, Eigenstructure-based coherence computations as an aid to 3-D structural and stratigraphic mapping: Geophysics, **64**, 1468–1479, doi: 10.1190/1.1444651.

Grewenig, S., J. Weickert, and A. Bruhn, 2010, From box filtering to fast explicit diffusion: Joint Pattern Recognition Symposium, Springer, 533–542.

Hale, D., 2009, Structure-oriented smoothing and semblance: CWP Report 635.

Hale, D., 2011, Structure-oriented bilateral filtering: CWP Report 695.

Hale, D., 2013, Methods to compute fault images, extract fault surfaces, and estimate fault throws from 3D seismic images: Geophysics, **78**, no. 2, O33–O43, doi: 10.1190/geo2012-0331.1.

Johnston, A. G., 2014, Interactions between the prograding Giant Foresets Formation and a subsiding depocentre: Insights from the Parihaka 3D & ES89 2D seismic surveys: Master's thesis, Victoria University of Wellington.

Lavialle, O., S. Pop, C. Germain, M. Donias, S. Guillon, N. Keskes, and Y. Berthoumieu, 2007, Seismic fault preserving diffusion: Journal of Applied Geophysics, **61**, 132–141, doi: 10.1016/j.jappgeo.2006.06.002.

Liu, Y., S. Fomel, and G. Liu, 2010, Nonlinear structure-enhancing filtering using plane-wave prediction: Geophysical Prospecting, **58**, 415–427, doi: 10.1111/(ISSN)1365-2478.

Ma, J., and G. Plonka, 2007, Combined curvelet shrinkage and nonlinear anisotropic diffusion: IEEE Transactions on Image Processing, **16**, 2198–2206, doi: 10.1109/TIP.2007.902333.

Marfurt, K. J., 2006, Robust estimates of 3D reflector dip and azimuth: Geophysics, **71**, no. 4, P29–P40, doi: 10.1190/1.2213049.

Marfurt, K. J., R. L. Kirlin, S. L. Farmer, and M. S. Bahorich, 1998, 3-D seismic attributes using a semblance-based coherency algorithm: Geophysics, **63**, 1150–1165, doi: 10.1190/1.1444415.

Marfurt, K. J., V. Sudhaker, A. Gersztenkorn, K. D. Crawford, and S. E. Nissen, 1999, Coherency calculations in the presence of structural dip: Geophysics, **64**, 104–111, doi: 10.1190/1.1444508.

Plonka, G., and J. Ma, 2008, Nonlinear regularized reaction-diffusion filters for denoising of images with textures: IEEE Transactions on Image Processing, **17**, 1283–1294, doi: 10.1109/TIP.2008.925305.

Randen, T., S. I. Pedersen, and L. Sønneland, 2001, Automatic extraction of fault surfaces from three-dimensional seismic data: 81st Annual International Meeting, SEG, Expanded Abstracts, 551–554.

Van Bemmel, P. P., and R. E. Pepper, 2000, Seismic signal processing method and apparatus for generating a cube of variance values: U.S. Patent 6,151,555.

Van Vliet, L. J., and P. W. Verbeek, 1995, Estimators for orientation and anisotropy in digitized images: Proceedings of the First Annual Conference of the Advanced School for Computing and Imaging ASCI'95, Heijen (The Netherlands), 442–450.

Weickert, J., 1997, A review of nonlinear diffusion filtering, *in* B. ter Haar Romeny, L. Florack, J. Koenderink, and M. Viergever, eds., Scale-space theory in computer vision: Springer Berlin Heidelberg, Lecture Notes in Computer Science 1252, 1–28.

Weickert, J., 1998, Anisotropic diffusion in image processing: Teubner Stuttgart.

Weickert, J., 1999, Coherence-enhancing diffusion filtering: International Journal of Computer Vision, **31**, 111–127, doi: 10.1023/A:1008009714131.

Weickert, J., 2001, Applications of nonlinear diffusion in image processing and computer vision: Acta Mathematica Universitatis Comenianae, **70**, 33–50.

Weickert, J., S. Grewenig, C. Schroers, and A. Bruhn, 2016, Cyclic schemes for PDE-based image analysis: International Journal of Computer Vision, **118**, 1–25.

Wu, X., 2017, Directional structure-tensor based coherence to detect seismic faults and channels: Geophysics, **82**, no. 2, A13–A17, doi: 10.1190/geo2016-0473.1.

Wu, X., and D. Hale, 2015, Horizon volumes with interpreted constraints: Geophysics, **80**, no. 2, IM21–IM33, doi: 10.1190/geo2014-0212.1.

Wu, X., and D. Hale, 2016a, 3D seismic image processing for faults: Geophysics, **81**, no. 2, IM1–IM11, doi: 10.1190/geo2015-0380.1.

Wu, X., and D. Hale, 2016b, Automatically interpreting all faults, unconformities, and horizons from 3D seismic images: Interpretation, **4**, no. 2, T227–T237, doi: 10.1190/INT-2015-0160.1.

Biographies and photographs of the authors are not available.